Available online at www.sciencedirect.com
SCIENCE DIRECT®
Journal of Solid State Chemistry 171 (2003) 161–169
JOURNAL OF SOLID STATE CHEMISTRY
http://elsevier.com/locate/jssc

Structural and magnetic characterization of $R\mathrm{CrO_4}$ oxides (R = Nd, Er and Tm)

R. Sáez-Puche,[a,*] E. Jiménez,[a] J. Isasi,[a] M.T. Fernández-Díaz,[b] and J.L. García-Muñoz[c]

[a] *Departamento Quimica Inorgánica I, Facultad de Ciencias Químicas, Universidad Complutense Madrid, Ciudad Universitaria, Madrid 28040, Spain*
[b] *Institut Laue-Langevin, 156X, Grenoble Cedex F-38042, France*
[c] *Instituto de Ciencias de Materiales de Barcelona, CSIC, Campus Universitari de Bellaterra, Bellaterra E-08193, Spain*

Received 13 May 2002; received in revised form 1 September 2002; accepted 17 November 2002

Abstract

The crystal and magnetic structure of $R\mathrm{CrO_4}$ oxides (R = Nd, Er and Tm) has been studied by owder neutron diffraction. These compounds crystallize with the zircon-type structure, showing tetragonal symmetry, space group $I4_1/amd$. In the case of $\mathrm{NdCrO_4}$, magnetic susceptibility measurements reveal the existence of an antiferromagnetic ordering in which both Cr^{5+} and Nd^{3+} sublattices are involved. This ordering has been explained on the basis of a propagation vector $k = 0$ and a collinear structure, described by the symmetry mode A_x, the ordered magnetic moments being 0.62 and 0.66 μ_B at 2 K for Nd^{3+} and Cr^{5+}, respectively. Magnetic susceptibility and magnetization measurements reveal that both $\mathrm{ErCrO_4}$ and $\mathrm{TmCrO_4}$ behave as ferromagnetic compounds with a Curie temperature of 15 and 18 K, respectively. Rietveld refinement of the neutron diffraction data for $\mathrm{ErCrO_4}$ yields a collinear magnetic structure described with an F_x mode. In the case of the $\mathrm{TmCrO_4}$ oxide, the ferromagnetic sublattices of Tm^{3+} and Cr^{5+} are aligned antiparallel in the $a-b$ plane, while along the c-axis the magnetic moments point to the same direction. In both compounds, the rather small values obtained for the Er^{3+} and Tm^{3+} ordered moments compared with the theoretical ones have been attributed to crystal field effects. The differences in the ferromagnetic structure of these compounds have been explained as the result of the higher rare-earth anisotropy of Tm^{3+} when compared with Er^{3+}, for which no magnetic component is present along the c-direction.

Keywords: Lanthanide chromates; Zircon-type structure; Neutron powder diffraction; Magnetic structure; Ferromagnetism; Antiferromagnetism

1. Introduction

The rare-earth compounds of general formula $RX\mathrm{O_4}$ (R = rare earth, X = P, V, As, Cr) crystallize in two structural types depending on the size of the rare-earth cation. The first member of the vanadates and chromates $\mathrm{La}X\mathrm{O_4}$, as well as the phosphate derivates where R = La–Tb and the arsenates with R = La–Nd, adopts the monazite-type structure, space group $P2_1/n$. The remaining oxides of these families of compounds crystallize with the zircon structural type, space group $I4_1/amd$ [1–3]. The latter structure can be described as built up by edges-sharing chains of distorted ($R\mathrm{O_8}$) bisdisphenoids running parallel to the a-axis, being connected one another by ($\mathrm{CrO_4}$) tetrahedra, as can be observed in Fig. 1. Recently, we have found that both $\mathrm{PrCrO_4}$ and $\mathrm{NdCrO_4}$ are dimorphic, showing the mentioned zircon type or the monazite structural type depending on the synthesis conditions [4]. However, the monazite polymorph has not been yet isolated as pure phase in the case of the $\mathrm{NdCrO_4}$ compound.

The existing detailed studies provide information about crystallographic phase transitions that occur in some of these compounds at low temperatures, coupled with magnetic and spectroscopic properties, mainly in the vanadate, phosphate and arsenate families [5–7]. For instance, a Jahn–Teller transition from tetragonal to orthorhombic symmetry has been vastly reported in the case of $\mathrm{TmVO_4}$ and $\mathrm{TmAsO_4}$ at a temperature of 2.15 and 6.0 K, respectively, the Tm^{3+} being a non-Kramer ion. Such transition is absent in the $\mathrm{TmPO_4}$ oxide, where the tetragonal symmetry is maintained in the whole range of temperatures, as the Tm^{3+} ground level is an

*Corresponding author. Fax: +34-91-3944352.
E-mail address: rsp92@quim.ucm.es (R. Sáez-Puche).

0022-4596/03/$ - see front matter © 2003 Elsevier Science (USA). All rights reserved.
doi:10.1016/S0022-4596(02)00203-7

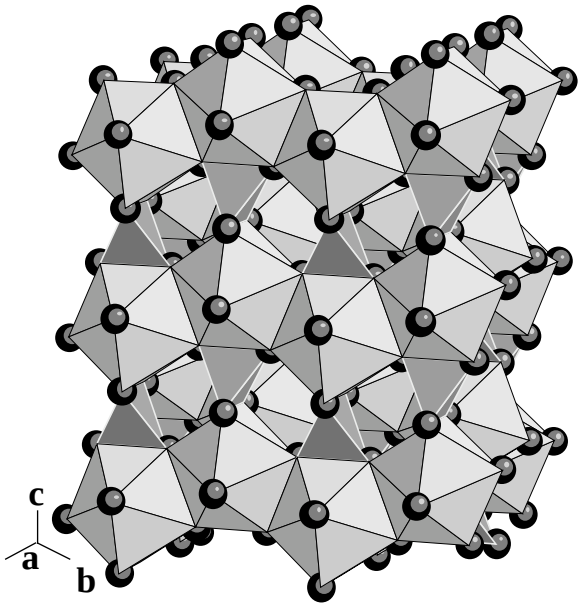

Fig. 1. Perspective view of the zircon-type structure, showing the chains of edge-sharing (RO_8) bisdisphenoids polyhedra, being connected by (CrO_4) tetrahedra units.

isolated singlet. Moreover, local random dynamic strains have been reported in the $TmAsO_4$ compound above 6.0 K. By contrast, only few studies have been reported concerning the $RCrO_4$ oxides. In this sense, only recently a tetragonal–orthorhombic transition has been observed by low-temperature X-ray experiments in the $DyCrO_4$ derivate [8].

The coexistence of two paramagnetic cations, namely Cr^{5+} and R^{3+}, in these $RCrO_4$ oxides constitutes a very interesting framework to study $3d-4f$ magnetic interactions and the predominant role that the rare-earth anisotropy plays in their magnetic properties. Most of these oxides have been reported as ferromagnets with Curie temperatures below 30 K [9]. However, our preliminary studies reveal that $SmCrO_4$, $EuCrO_4$ and $LuCrO_4$ behave as antiferromagnets [10]. The remaining members of this series show a rich variety of magnetic phenomena. The aims of this work are the crystallographic characterization of the $RCrO_4$ compounds (R = Nd, Er and Tm) by both X-ray and neutron diffraction techniques, and the subsequent study of their magnetic properties from magnetic susceptibility, magnetization and neutron diffraction data obtained at different temperatures.

2. Experimental

The samples were prepared as pure phases by heating the stoichiometric amounts of $R(NO_3)_3 \cdot 6H_2O$ and $Cr(NO_3)_3 \cdot 9H_2O$, following the thermal scheme: 30 min at 433 K, 30 min at 473 K and 60 min at 773 K. An oxygen flow has been used in order to stabilize the unusual 5+-oxidation state of the chromium ion. The reaction takes place according to

$$R(NO_3)_3 \cdot 6H_2O + Cr(NO_3)_3 \cdot 9H_2O \xrightarrow{O_2} RCrO_4 + 6NO_2 + 15H_2O$$

The obtained compounds are dark green colored.

The neutron powder diffraction experiments were carried out using the High Flux Reactor facilities of the Institute Laue Langevin (Grenoble, France). The data, collected using the medium-resolution D1B diffractometer ($\lambda = 2.5251$ Å), permit to study the thermal evolution of the neutron patterns of the different samples in the temperature range between 2 and 100 K over an angular range of $15^\circ < 2\theta < 95^\circ$ with steps of 0.2°. All data were analyzed with the Rietveld method using the FULLPROF program [11]. A pseudo-Voigt profile function has been used to describe the peak shape. In all cases, an impurity around $2\theta = 72^\circ$, due to the sample holder, has been detected in the neutron diffraction patterns.

Magnetic susceptibility measurements were performed in a Quantum Design XL-SQUID magnetometer in the temperature range of 1.9–300 K at different applied magnetic fields. The susceptibilities were corrected for ionic diamagnetism [12]. The magnetization was measured at different temperatures in the magnetic field range of 0–5 T.

3. Results and discussion

3.1. Structural characterization

X-ray and neutron diffraction data reveal that all the samples are isostructural, having been refined according to the zircon-type structure, SG $I4_1/amd$. The structural parameters obtained from the Rietveld refinement are shown in Table 1. R^{3+} ions are placed in 4*a* sites (0, 3/4, 1/8), Cr^{5+} in 4*b* sites (0, 1/4, 3/8) and the oxygen in 16*h* sites $(0, y, z)$. The main d(Cr–O) and d(R–O) distances are also included in Table 1. The rare-earth ions are centered in their respective distorted bisdisphenoids in an octa-coordination, while the coordination of the chromium ion is tetrahedral. The size of the (RO_8) bisdisphenoid polyhedra diminish progressively along with the size of the R^{3+} ion from Nd^{3+} to Tm^{3+}, while the size of the (CrO_4) tetrahedra evolves in the opposite direction. This fact can be explained taking into account the competition to form the R–O and Cr–O bonds. The smaller size of the R^{3+} ion yields a more acidic Lewis character, thereby presenting more affinity for the electrons in the R–O bonds. Consequently, the Cr–O bonds become weaker, justifying the progressive increase of the Cr–O distance along the $RCrO_4$ series of

Table 1
Lattice parameters, atomic oxygen coordinates and conventional discrepancy factors from Rietveld refinement of neutron diffraction data obtained at 50 K for $RCrO_4$ (R = Nd, Er and Tm) oxides

R	a (Å)	c (Å)	y	z	R_{wp}	R_B	d(Cr–O) (Å)	d(R–O) (Å)
Nd	7.266(8)	6.358(3)	0.428(7)	0.202(2)	7.03	3.30	1.701(1) × 4	2.452(8) × 4 2.385(7) × 4
Er	7.055(2)	6.193(8)	0.436(2)	0.197(5)	11.9	4.80	1.713(2) × 4	2.390(8) × 4 2.258(9) × 4
Tm	7.032(2)	6.181(9)	0.437(5)	0.197(6)	10.7	4.99	1.715(1) × 4	2.390(7) × 4 2.242(9) × 4

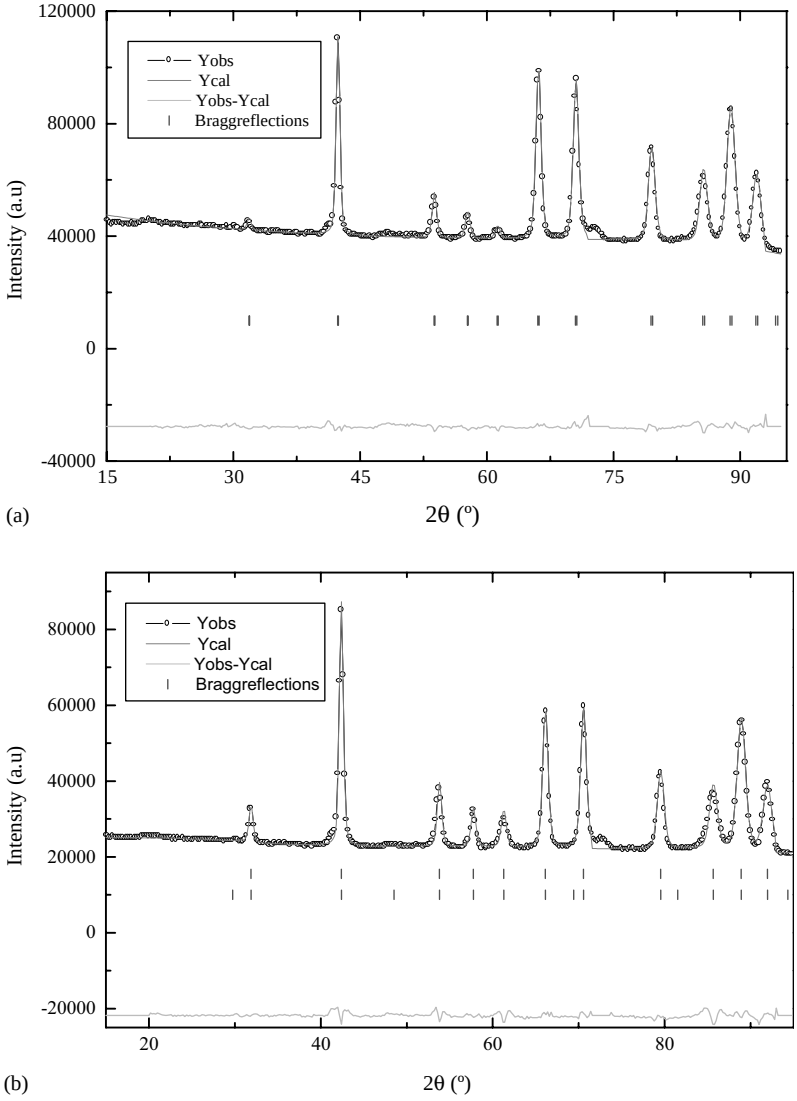

Fig. 2. Refined neutron diffraction pattern for the $TmCrO_4$ compound at 100 K (a) and at 2 K (b); second row of vertical marks in (b) correspond with the magnetic reflections.

oxides. According to the above discussion, the a and c lattice parameters of these phases decrease linearly with the reduction of the ionic radius of the rare earth from Nd to Tm, due to the lanthanide contraction. Fig. 2a shows the refined neutron diffraction pattern obtained at 100 K for $TmCrO_4$.

3.2. Magnetic properties

The temperature dependence of the molar magnetic susceptibility for $ErCrO_4$ and $TmCrO_4$ at different fields is shown in Figs. 3 and 4. The experimental data follow a Curie–Weiss behavior, $\chi = C/(T-\theta)$, in a wide range

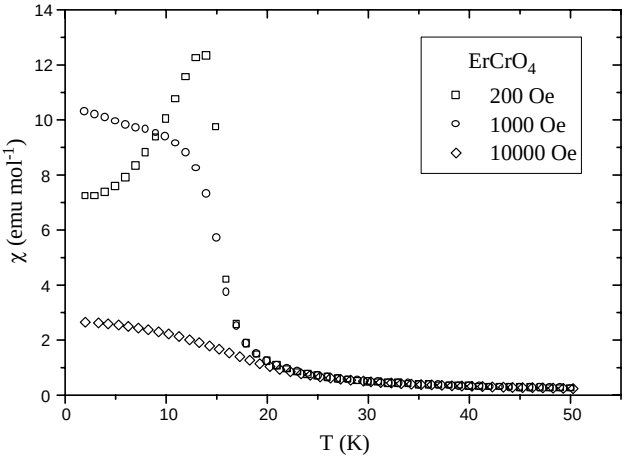

Fig. 3. ZFC magnetic susceptibility of the $ErCrO_4$ phase at different magnetic fields.

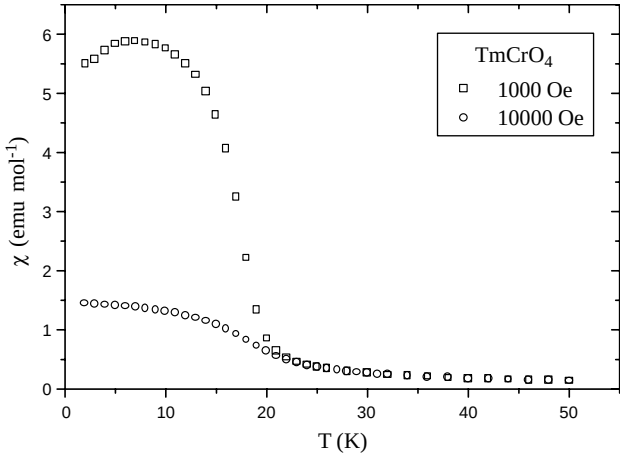

Fig. 4. Variation of the magnetic susceptibility with the temperature for the $TmCrO_4$ oxide.

of temperatures 300–50 K, in both cases. The obtained values of the effective magnetic moment after discounting the Cr^{5+} contribution, 1.66 μ_B taken from $LuCrO_4$ [10], are 9.6 and 7.6 μ_B for Er^{3+} and Tm^{3+}, respectively, what agrees with the theoretical ones calculated by the Hund's equation, see Table 2. However, at temperatures below 50 K, the magnetic behavior of these samples depends on the particular rare-earth cation present in each $RCrO_4$ oxide. Besides that, the magnetic susceptibility becomes field dependent. The values of the Weiss constant, see Table 2, and the sudden increase observed in the susceptibility at 25 K (Er) and 20 K (Tm) can be attributed to ferromagnetic interactions in the Cr^{5+} and R^{3+} sublattices. The maxima observed at low magnetic fields can be ascribed to the random orientation of magnetic domains, what reduces considerably the overall magnetization of the sample.

Table 2
Magnetic data for the $RCrO_4$ oxides (R = Nd, Er and Tm): experimental magnetic moment (μ_{exp}), Weiss constant (θ), ordering temperature (T_c), coercitive field (H_c), remanence (M_r) and saturation magnetization (M_s)

Compound	μ_{exp} (μ_B)[a]	θ (K)	T_c (K)	H_c (Oe)	M_r (μ_B)	M_s (μ_B)
$NdCrO_4$	4.06	−45.5	25 (Ref. [8])	—	—	—
$ErCrO_4$	9.60	9.01	15	275	0.71	6.0
$TmCrO_4$	7.58	−6.82	18	1100	1.37	3.97

[a] After discounting the Cr^{5+} magnetic contribution.

The temperature dependence of the reciprocal molar magnetic susceptibility between 2 and 300 K for $NdCrO_4$ is shown in Fig. 5. The magnetic susceptibility in this oxide obeys the Curie–Weiss law from 300 to 50 K approximately. The downwards deviation in the χ^{-1} vs. T observed below 20 K and the negative value of the Weiss constant ($\theta = -45.5$ K) can be ascribed to antiferromagnetic interactions and/or crystal field effects. Similar results have been reported earlier for different neodymium oxides where co-operative interactions are not present [13]. However, the small value of χT obtained at 2 K (Fig. 5, inset), which is only 0.11 emu K mol^{-1}, indicates that incipient antiferromagnetic interactions appear to be operative at low temperature.

Hysteresis loops from −5 to 5 T below the Curie temperature, i.e. 2 K, have been measured for $ErCrO_4$ and $TmCrO_4$, see Figs. 6 and 7. In both cases, characteristic cycles of ferromagnetic materials have been obtained. The remanence and coercitive field are higher for the $TmCrO_4$ compared with the $ErCrO_4$, due to the higher anisotropy associated to the Tm^{3+} with respect to the Er^{3+} cation, what is evidenced in a higher second-order Stevens coefficient. Furthermore, it is important to observe that the flux density continues to increase beyond the saturation magnetic polarization at 2000 and 6000 Oe for the $ErCrO_4$ $TmCrO_4$, respectively. Such increase stems from the Zeeman splitting of the crystal field states, together with a remarkable mixture of the eigenfunctions of the corresponding states, caused by the applied magnetic field. These crystal field states must be relatively close in energy, so that the mixture can be effective and experimentally observable. Such effects cause a continuous variation of the magnetic contribution arising from the rare-earth sublattice. The magnetization values obtained at the higher magnetic field strength of 5 T in both cases are approximately 50 per cent of the theoretical ones expected for these two rare-earth cations, as can be observed in Figs. 6 and 7.

In the case of the $ErCrO_4$ and $TmCrO_4$, neutron diffraction experiments at different temperatures between 100 and 2 K reveal the progressive increase of the intensity of certain reflections below the Curie temperature when the temperature decreases. However, as can

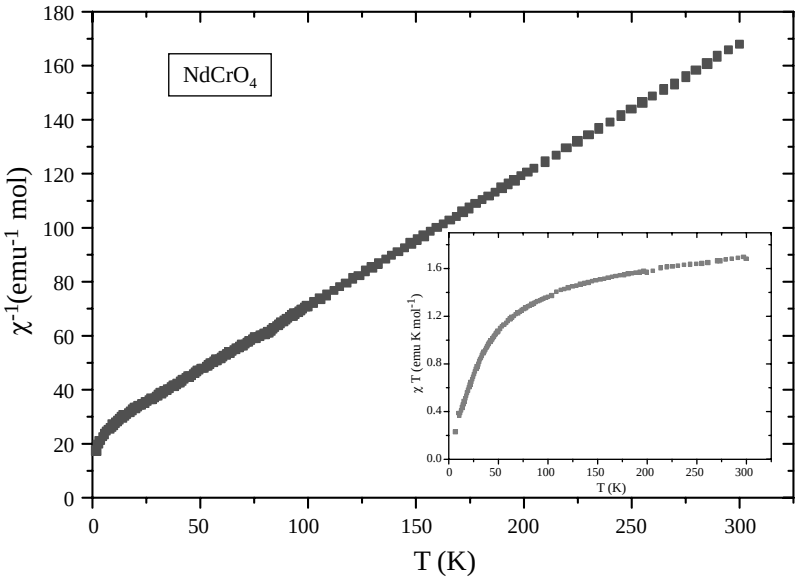

Fig. 5. Reciprocal magnetic susceptibility as a function of the temperature for the $NdCrO_4$ oxide between 2 and 300 K at 100 Oe. The inset corresponds with the χT vs T plot.

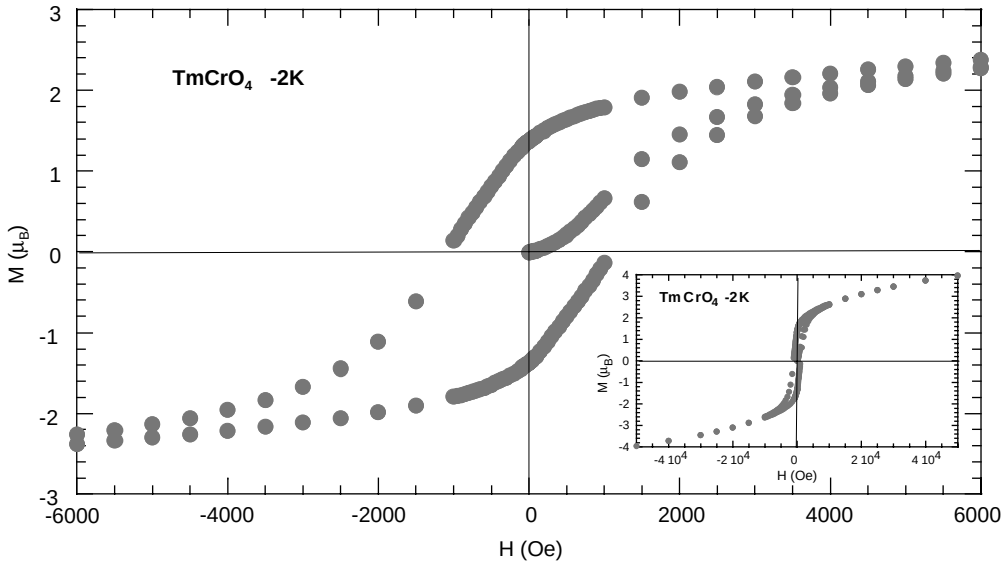

Fig. 6. Hysteresis loop from −5 to 5 T for the $ErCrO_4$ compound at 2 K.

be observed in both cases in Figs. 2 and 8, no extra reflections have been observed in the low-temperature patterns [14]. These magnetic reflections have been indexed on the basis of a propagation vector $k = (000)$. The basis vector components for the irreducible representation, which could describe the magnetic order for the Cr^{5+} and R^{3+} sublattices, can be obtained from the representation analysis method proposed by Bertaut [15].

In these $RCrO_4$ oxides, four atoms are present in each magnetic sublattice inside the unit cell. However, two of such atoms are immediately generated by the application of the translation operator t (1/2,1/2,1/2) to the other two atoms. That symmetry operator does not alter the direction of the magnetic moments. Therefore, only two atoms in each magnetic sublattice are to be considered when carrying out the representation analysis and describing the magnetic structure of the rare-earth chromates. The basis vectors are constructed from the linear combination of the spin components of the chromium and rare-earth atoms, as both sublattices become magnetically coupled below the ordering temperature.

Rietveld refinement of the powder neutron diffraction data obtained at 2 K for $ErCrO_4$, see Fig. 8, shows that the best fit regarding the magnetic reflections is obtained

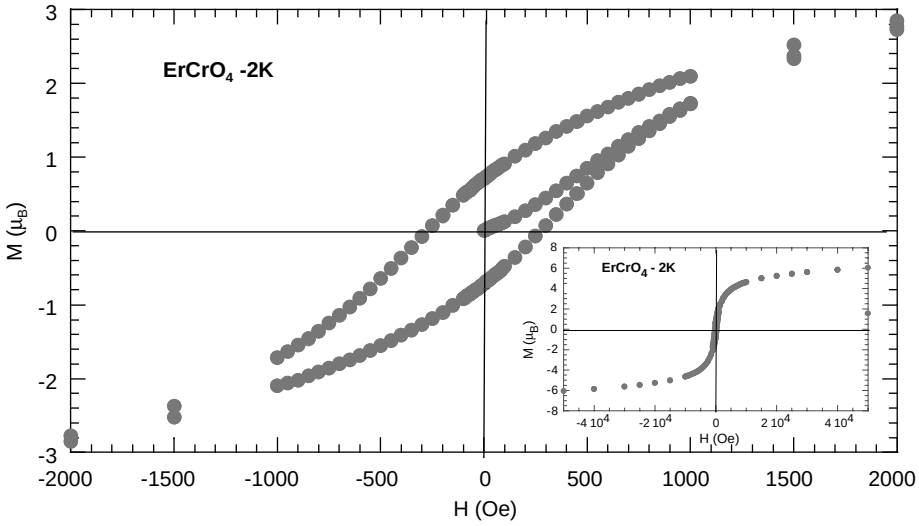

Fig. 7. Hysteresis loop from −5 to 5 T for the $TmCrO_4$ compound at 2 K.

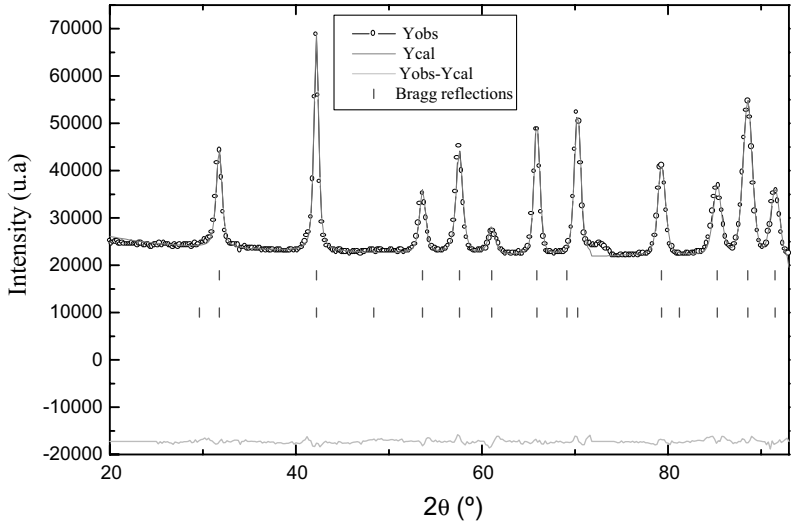

Fig. 8. Neutron diffraction pattern of the $ErCrO_4$ oxide at 2 K; first and second rows of vertical marks correspond with the nuclear and magnetic reflections, respectively.

with an F_x magnetic mode, where both magnetic sublattices are strongly coupled generating a collinear structure, Fig. 9. The obtained ordered magnetic moments take values of 0.91 and 5.09 μ_B for Cr^{5+} and Er^{3+} respectively, see Table 3. A relatively small experimental value is obtained for the magnetic moment of the Er^{3+} ions compared with the theoretical one ($gJ = 9\,\mu_B$), which could be attributed to crystal field effects that may cause a partial quenching of the angular moment associated with the Er^{3+} ion. The orientation of the magnetic components in the *ab*-plane cannot be unambiguously determined by powder neutron diffraction experiments in these tetragonal compounds when they present a collinear magnetic structure, because all orientations are energetically equivalent for a specific spin configuration.

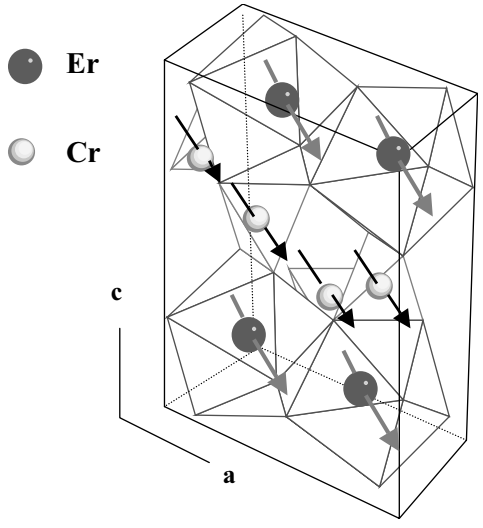

Fig. 9. Magnetic structure of the $ErCrO_4$ oxide at 2 K.

Fig. 2b shows the neutron diffraction pattern of $TmCrO_4$ obtained at 2 K and refined considering F_xF_z magnetic modes. The two ferromagnetic sublattices are aligned antiparallel in the *ab*-plane, while their magnetic moments lie in the same direction along the *c*-axis. The values of the ordered magnetic moments obtained in the Rietveld refinement are 1.14 and 3.13 μ_B for Cr^{5+} and Tm^{3+}, respectively, their larger component lying along the *c*-direction, Fig. 10. When the theoretical ($gJ = 7\,\mu_B$) and the experimental (3.13 μ_B) values obtained for Tm^{3+} ion are compared, one can see that the latter is between the spin-only and spin–orbit values. This fact suggests that the orbital momentum is partially quenched by the crystal field, as in the case of the Er^{3+} ion. On the other hand, the magnetic moment of the Cr^{5+} ions is somewhat higher than the spin-only value ($2S = 1\,\mu_B$), implying the existence of some orbital contribution, which will provide some anisotropy to the Cr^{5+} ions. As a consequence, a competition between the R^{3+}–Cr^{5+} interactions and the anisotropy will take place in these chromates. The inclination of the magnetic moments with respect to the *ab*-plane in $TmCrO_4$ may be the result of a higher rare-earth anisotropy when compared with $ErCrO_4$, where no magnetic components are present in the *c*-direction.

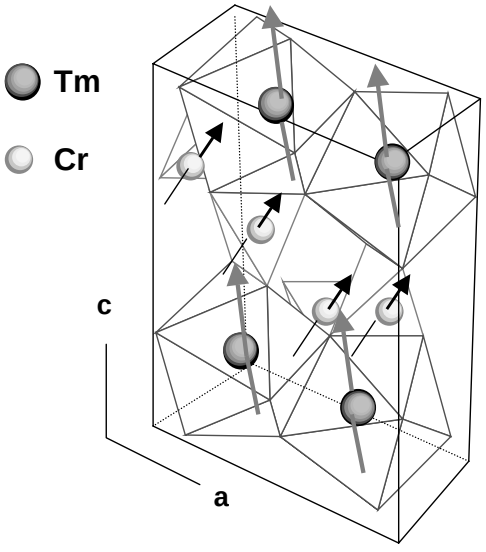

Fig. 10. Magnetic structure of the $TmCrO_4$ oxide at 2 K.

Fig. 11 shows the refined neutron diffraction data at 2 K for the $NdCrO_4$ oxide. The occurrence of new reflections at 2 K compared with the data obtained at higher temperatures, together with the increase in intensity of some nuclear reflections at this low

Table 3
$RCrO_4$:magnetic ions in the unit cell together with the corresponding magnetic moments (μ_B) at 2 K

Atom (site)	$NdCrO_4$			$ErCrO_4$			$TmCrO_4$		
	M_x	M_z	M_T	M_x	M_z	M_T	M_x	M_z	M_T
*R*1 (0, 3/4, 1/8)	0.62	—	0.62	5.09	—	5.09	−0.28	3.12	3.13
*R*2 (0, 1/4, 7/8)	−0.62	—	0.62	5.09	—	5.09	−0.28	3.12	3.13
Cr1 (0, 1/4, 3/8)	0.66	—	0.66	0.91	—	0.91	0.63	0.94	1.14
Cr2 (0, 3/4, 5/8)	−0.66	—	0.66	0.91	—	0.91	0.63	0.94	1.14
	$R_{mag} = 10.24$			$R_{mag} = 3.39$			$R_{mag} = 3.75$		

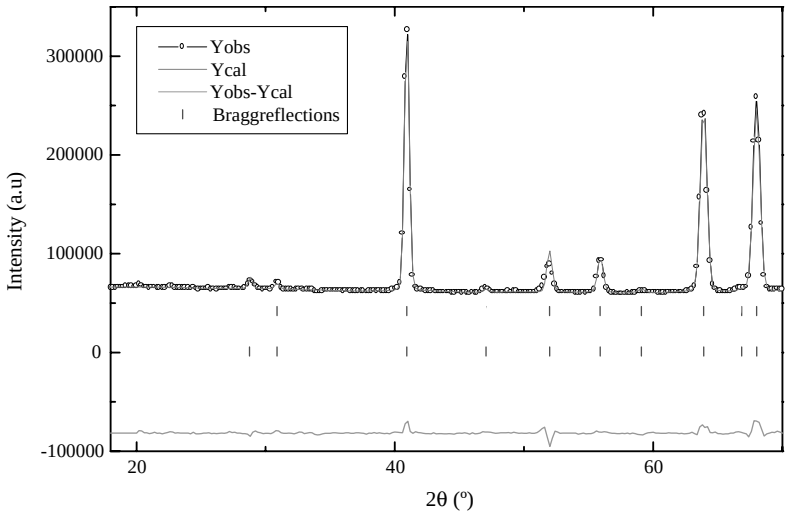

Fig. 11. Neutron diffraction data obtained at 2 K for the $NdCrO_4$ oxide; first and second rows of vertical marks correspond with the nuclear and magnetic reflections, respectively.

temperature, can be clearly appreciated. These Bragg reflections can be indexed with a propagation vector $k = (000)$, as in the case of the isostructural $TmCrO_4$ and $ErCrO_4$ compounds, whose magnetic structure has been described above. However, taking into account the magnetic susceptibility data, it is possible to leave out the ferromagnetic modes. The best fit of the experimental data is obtained for an A_x magnetic mode, yielding a collinear structure in which both Cr^{5+} and Nd^{3+} are coupled with their magnetic moments aligned in the *ab*-plane, with no contribution in the *c*-axis (see Fig. 12). The obtained magnetic moment for Cr^{5+} of $0.66\,\mu_B$ is smaller than the expected $2S = 1\,\mu_B$. The value of the Nd^{3+} magnetic moment ($0.62\,\mu_B$) is much lower than the theoretical $gJ = 3.27\,\mu_B$ corresponding to this Kramers ion with a $^4I_{9/2}$ ground state. This result agrees with the magnetic susceptibility measurements, where the deviations from the linearity in the χ^{-1} vs T plot (Fig. 5) are larger than those expected taking into account only the crystal field splitting effects. Recently, a T_N value of 25 K has been reported from specific heat measurements [8]. The antiferromagnetic interactions in the Nd^{3+} sublattice are induced by the polarization of the antiferromagnetically ordered Cr^{5+} ions. At 2 K, the saturation state has not been reached in either of the magnetic sublattices. Neutron diffraction experiments below 2 K are now in progress in order to study the evolution of the ordered magnetic moments until saturation is reached.

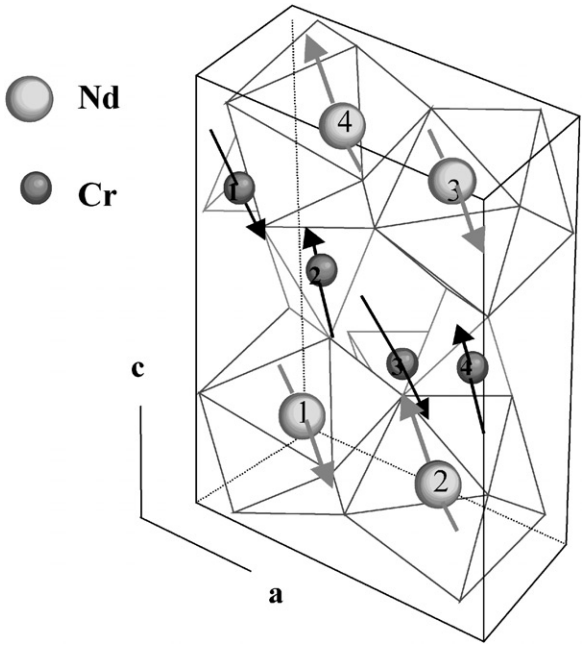

Fig. 12. Magnetic structure of the $NdCrO_4$ oxide at 2 K.

Furthermore, a careful analysis of the evolution of the neutron diffraction patterns with the temperature in the case of R = Nd and Tm reveals a remarkable broadening of some reflections when temperature is above but close to the ordering temperature, see Fig. 13. By contrast, below such ordering temperature no further broadening has been detected. These facts may be due to a structural phase transition above the magnetic ordering temperature. The fact that such phenomenon is observed in $NdCrO_4$, where the Nd^{3+} is a Kramers ion, suggests a

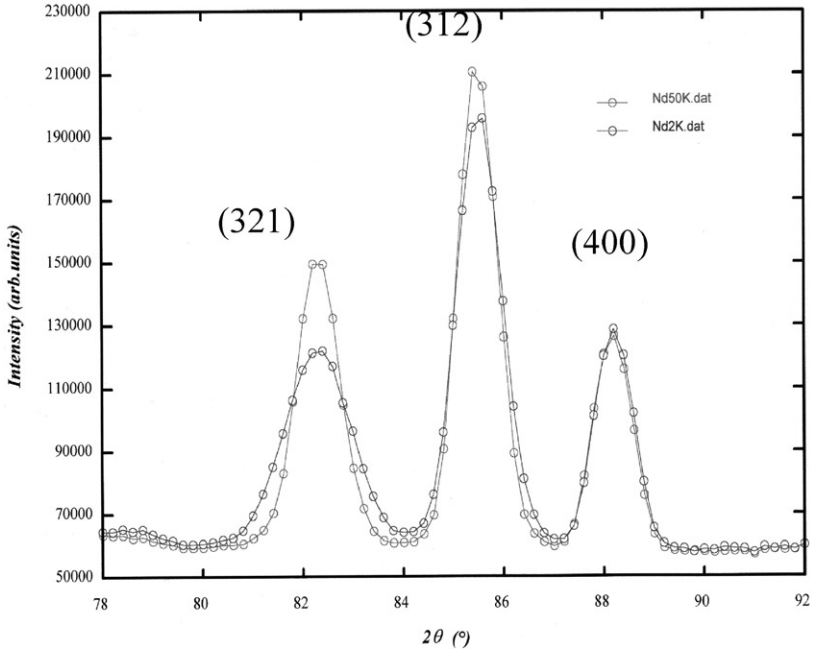

Fig. 13. Neutron diffraction pattern at 2 and 50 K for the $NdCrO_4$ compound between 78° and 92°. A noticeably broadening can be observed in the reflections (321) and (312), while the (400) remains unchanged.

possible role of the Cr^{5+} ions in the phase transition. Magnetoelastic effects, associated with the polarization of these magnetic ions above T_N, could generate anisotropic strains in the tetragonal lattice. It is worth mentioning that recently a tetragonal–orthorhombic transition has been observed by low-temperature X-ray experiments in the $DyCrO_4$ compound [8]. This low-temperature orthorhombic phase presents a space group *Imma*. Such transition, that may also take place in the $NdCrO_4$ and $TmCrO_4$ oxides, implies a shift of the oxygen atoms from their atomic positions in the tetragonal phase, the rare earth and chromium atoms remaining in their original positions. Therefore, the topology of the lattice will not be altered through the structural transition. Further neutron diffraction work is now in progress in order to study such tetragonal–orthorhombic transition.

Acknowledgments

We thank DGICYT for financial support, under the Project MAT-2000-0753-C02-01, and Dr. J Rodriguez-Carvajal (LLB, Saclay, France) for useful and valuable discussions. The ILL and the CICYT (funding of D1B-CRG) are acknowledged for beam provision.

References

[1] V.H. Schwarz, Z. Anorg. Allg. Chem. 322 (1963) 1;
V.H. Schwarz, Z. Anorg. Allg. Chem. 323 (1963) 45.
[2] G. Buisson, F. Bertaut, J. Mareschal, C. R. Acad. Sci. Paris. 259 (1964) 411.
[3] J.D. Carter, H.U. Anderson, M.G. Shumsky, J. Mater. Sci. 31 (1996) 551.
[4] E. Jiménez, J. Isasi, R. Sáez-Puche, J. Alloys Compds. 323–324 (2001) 115.
[5] J.A. Hodges, P. Imbert, G. Jéhanno, J. Phys. 43 (1982) 1249.
[6] P.J. Becker, G.A. Gehring, J. Phys. C: Solid State Phys. 14 (1981) 1945.
[7] J.H. Page, D.R. Taylor, S.R.P. Smith, J. Phys. C: Solid State Phys. 17 (1984) 51.
[8] K. Tezuka, Y. Hinatsu, J. Solid State Chem. 160 (2001) 362.
[9] H. Walter, H.G. Kahle, K. Mulder, H.C. Schopper, H. Schwarz, Int. J. Magn. 5 (1973) 129.
[10] E. Jiménez, J. Isasi, R. Sáez-Puche, J. Alloys Compds. 312 (2000) 53.
[11] J. Rodríguez-Carvajal, in: Abs. of the Satellite Meeting on Powder Diffraction of XVth, Congress of the International Union of Crystallography, Toulouse, 1990, p. 127.
[12] L.N. Mulay, E. Boudreaux, Theory of Molecular Paramagnetism, Wiley, New York, 1976, p. 494.
[13] J. Romero de Paz, J. Hernandez Velasco, M.T. Fernández-Díaz, P. Porcher, J.L. Martínez, R. Sáez Puche, J. Solid State Chem. 148 (1999) 361.
[14] E. Jiménez, J. Isasi, R. Sáez-Puche, J. Alloys Compds. 344 (2002) 369.
[15] E.F. Bertaut, Acta Crystallogr. A 24 (1968) 217.